https://doi.org/10.5194/hess-2022-330
Preprint. Discussion started: 4 October 2022

Hydrology and Earth System Sciences
Discussions

Impact of urban geology on shallow groundwater

Ane LaBianca[1,2], Mette H. Mortensen[1], Peter Sandersen[1], Torben O. Sonnenborg[1], Karsten H. Jensen[2], Jacob Kidmose[1]

[1]Geological Survey of Denmark and Greenland (GEUS), Copenhagen, Denmark
[2]Department of Geosciences and Natural Resource Management, University of Copenhagen, Copenhagen, Denmark

Correspondence to: Ane LaBianca (ala@geus.dk)

Abstract. This study examines the impact of urban geology and spatial resolution on the simulation of shallow groundwater levels and flows at the city scale. The study uses an integrated hydrological model based on the MIKE SHE code that couples surface water and 3D groundwater simulations with a leaky sewer system. The effect of geological configuration was analyzed by applying three geological models to an otherwise identical hydrological model. The effect of spatial resolution was examined by using two different horizontal grid sizes in the hydrological model, respectively 50 m and 10 m. The impact of the geological configuration and spatial resolution was analyzed based on model calibration, simulations of high-water levels, and particle tracking. The results show that a representation of the subsurface infrastructure, and near terrain soil types, in the geological model impacts the simulation of the high-water levels when the hydrogeological model is simulated in 10 m resolution. This was detectable even though the difference between the geological models only occurs in 7% of the volume of the geological models. When the hydrological model was run in 50 m horizontal resolution, the impact of the urban geology on the high-water levels was smeared out. Results from particle tracking show that representing the subsurface infrastructure in the hydrological model changed the particles' flow path and travel time to sinks, both in the 50 m and 10 m horizontal resolution of the hydrological model. It caused less recharge to deeper aquifers and increased the percentage of particles flowing to saturated zone drains and leaky sewer pipes. In conclusion, the results indicate that even though the subsurface infrastructure and fill material only occupy a small fraction of the shallow geology, it affects the simulation of local water levels and substantially alters the flow paths. The comparison of the spatial resolution demonstrates that to simulate this effect the spatial resolution needs to be of a scale that represents the local variability of the shallow urban geology.

1 Introduction

As more than half of the world's population lives in urban areas and urbanization globally continues to increase (United Nations, 2018), urban water resources receive increasing attention (McGrane, 2016; Lundy and Wade, 2011; Mitchell, 2006; Farr et al., 2017; Birks et al., 2013). The main factors which impact the urban hydrological system are the impervious land cover, upper soil alterations, subsurface infrastructure, and groundwater abstraction. These factors alter the natural set of flow paths and create artificial supply and sewer pathways (Salvadore et al., 2015; Schirmer et al., 2013; McGrane, 2016).

https://doi.org/10.5194/hess-2022-330
Preprint. Discussion started: 4 October 2022


Hydrology and Earth System Sciences
Discussions

Cities are hydrologically complex, because of interactions between urban structures, piped water networks, and the natural hydrological system, with surface and subsurface processes occurring at various spatial and temporal scales (Salvadore et al., 2015; Han et al., 2017; Kidmose et al., 2015; Fletcher et al., 2013; Tubau et al., 2017; Vázquez-Suñé et al., 2016; McGrane, 2016).

In urban areas, shallow geology is more extensively moderated than in rural areas, both in its physical extent and in the temporal frequency of alteration. This is a consequence of the high population density, which generates the development of high concentrations of buildings and physical infrastructure as well as transport and utility networks (Attard et al., 2016b; Lerner, 1990, 2002). This shallow geology, which is highly affected by man is also referred to as the anthropogenic layer (Mielby and Sandersen, 2017; Ford et al., 2014). The anthropogenic layer can vary in extent and composition within a few meters. Furthermore, the composition and properties of the anthropogenic layer change frequently in urban areas because of the reconstruction of the land surface, maintenance of existing subsurface installations, or new underground constructions (Salvadore et al., 2015; Fletcher et al., 2013; Hibbs and Sharp, 2012; Berthier et al., 2004; Ford et al., 2014). Mielby and Sandersen (2017) argue that it is important to know the city's history to quantify the anthropogenic layer and suggest that different modeling approaches are required for the anthropogenic material and the underlying geological sediments respectively for developing a combined subsurface model.

Previous studies have highlighted that the hydraulic characteristics of the anthropogenic layer can cause preferential flow pathways (Salvadore et al., 2015; Fletcher et al., 2013; Berthier et al., 2004) and that underground structures may act as obstacles to flow (Hibbs and Sharp, 2012; Lerner, 1990, 2002; Pophillat et al., 2022) and increase mixing of shallow and deep aquifers (Attard et al., 2016b, 2017). Yet, only a few studies have considered the impact of anthropogenic modifications on the groundwater flow when modeling urban hydrogeology at the city scale (Berthier et al., 2004; Attard et al., 2017). Berthier et al. (2004) considered the anthropogenic modifications of soils in a 2D numerical model setup. They found that the soil hydraulic conductivities have a significant impact on water table level and runoff from drained layers. However, the model was only applied to a small area (0.05 km^2) and neglected evapotranspiration and infiltration on paved surfaces. Moreover, often urban hydrogeological models mainly focus on the impact of the subsurface close to a specific construction site (Mielby and Sandersen, 2017; Laursen and Linderberg, 2017; Attard et al., 2016b; Troldborg et al., 2021). Yet, studies by Attard et al. (2016b, 2017), Boukhemacha et al. (2015), and Epting et al. (2008) show examples of studies that use numerical modeling to quantify the cumulative impact and interaction of multiple underground structures on the groundwater flow. These studies found that urbanization impacts the water balance and flow systems both at local and larger scales. However, they mainly focused on obstacles to the flow and did not consider the entire local heterogeneity of the subsurface properties (Hibbs and Sharp, 2012; Attard et al., 2016b, a, 2017; Locatelli et al., 2017).

Comprehensive numerical groundwater models require detailed geological input. For the shallow urban subsurface, a detailed spatial description of the landcover and the geological settings down to a scale of a few meters is required, Salvadore et al. (2015), Hutchins et al. (2017) and Mielby and Sandersen (2017). This increases the effort needed to compile and process large amounts of data including the temporal changes of the urban subsurface compared to traditional

https://doi.org/10.5194/hess-2022-330
Preprint. Discussion started: 4 October 2022


Hydrology and Earth System Sciences
Discussions

hydrogeological modeling (Salvadore et al., 2015; Hutchins et al., 2017). Models of shallow urban geology thus require data that is normally not used in hydrogeological models, such as the location of the subsurface infrastructure and buildings, and descriptions of back-fill material. Growing urbanization makes it increasingly difficult to survey the urban subsurface (Petrosino et al., 2021; Culshaw and Price, 2011; Mielby and Sandersen, 2017), and high spatial variability of the subsurface and sparse data introduce high uncertainty to the modeling (Salvadore et al., 2015). Nevertheless, studies by Andersen et al. (2020), Mielby and Sandersen (2017) and Vázquez-Suñé et al. (2016) have introduced methods of compiling subsurface data from various sources and developing 3D geological models of the urban subsurface.

Integrated hydrological modeling of urban hydrology favors the ability to address the entire array of hydrological processes within urban areas (Hutchins et al., 2017; Rodriguez et al., 2008). Laursen and Linderberg (2017) and Mielby and Henriksen (2020) argue that integrated models of the surface and subsurface processes at the city scale, which can give reliable estimations of consequences of potential changes, are needed for effective urban water resources management. Current integrated surface-subsurface modeling of urban hydrology however often simplifies the description of the subsurface components (Pophillat et al., 2021). Yet, while simple models might describe the impact of the subsurface on the surface hydrology acceptably, processes and interactions affecting the water cycle and the subsurface flow system in the presence of a shallow groundwater table may be neglected (Pophillat et al., 2021; Attard et al., 2016c). Common limitations of integrated modeling are data shortage, undescribed processes, and parameterization, which all are sources of uncertainty (Salvadore et al., 2015; Schirmer et al., 2013; Pophillat et al., 2021; Fletcher et al., 2013).

Models of the urban hydrological system at the city scale are typically challenged by the presence of leaking water pipes or sewers that cause unintended groundwater recharge or drainage. The location and to which degree the pipes are leaking are often poorly documented (Lerner, 2002; Yang et al., 1999; Hibbs and Sharp, 2012; Tubau et al., 2017; Vázquez-Suñé et al., 2010), and climatic and hydrological observations are often sparse (Fletcher et al., 2013; Salvadore et al., 2015; Hutchins et al., 2017; McGrane, 2016). Yet, Hutchins et al. (2017) highlighted that the advances in monitoring techniques, digitalization, and computational power have created an opportunity to build complex integrated hydrological models with reduced uncertainty.

Previous studies have shown that the urban subsurface is highly complex, with preferential flow paths due to anthropogenic fill material and flow barriers due to subsurface buildings (Salvadore et al., 2015; Hibbs and Sharp, 2012; Lerner, 2002, 1990), but few studies have documented the effects of the anthropogenic layer on groundwater at city scale. Moreover, even fewer studies use integrated modeling considering both surface and groundwater flows and their interaction with leaking water pipes and sewers. Integrated models of the surface and subsurface processes at the city scale are however needed for effective urban water resources management (Laursen and Linderberg, 2017; Mielby and Henriksen, 2020; Hutchins et al., 2017).

This study investigates the impact of anthropogenic urban geology and spatial resolution on the simulation of shallow groundwater levels and flows at the city scale using an integrated hydrological model based on the MIKE SHE code. The Danish city of Odense is used as the case study for the model experiment. The objectives are (1) to develop two models of

https://doi.org/10.5194/hess-2022-330
Preprint. Discussion started: 4 October 2022

Hydrology and Earth System Sciences
Discussions

the urban geology, (2) to set up a hydrological model that integrates the surface-groundwater processes, as well as interactions with the sewer system, (3) to analyze the effect of the geological models on the simulation of groundwater levels and flow, and (4) to analyze the effect of computational grid size on the simulations.

2 Site description

The city of Odense is located near the coast in the south-central part of Denmark (Figure 1). The city dates back to 1580 and has mainly expanded since the beginning of the 19th century (Laursen and Linderberg, 2017). Figure 1 shows the areal extent of the model domain, which covers 9.8 km^2 and is an urban area that was developed in the 1960s-70s (Mielby and Sandersen, 2017). Within the model domain, the terrain slopes from the west towards the northeast, with elevations from 45 to 5 meters above sea level (m.a.s.l.). There is one creek in the model named Hedebækken, see Figure 1a, which intersects the model boundary in the west and flows into the Odense River towards the east. Odense River makes up the eastern boundary of the model domain. Previous bog and marshland in the area have been drained and to a large degree urbanized since the 1950s (Laursen and Linderberg, 2017).

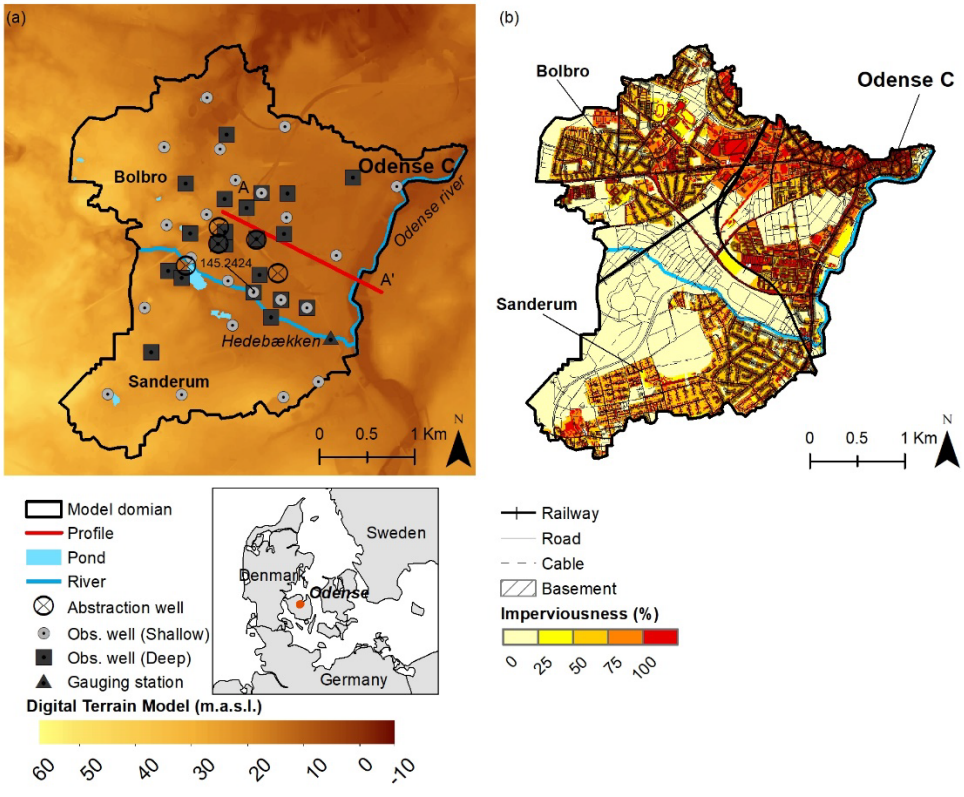

Figure 1. Maps of the model domain, a part of the city of Odense, Denmark. Panel (a) displays a digital terrain model from the Danish National Agency for Data Supply and Infrastructure (2019) with locations of observation points and abstraction wells provided by Vandcenter Syd A/S (2021). Panel (b) depicts the imperviousness retrieved from Vandcenter Syd A/S (2019a) and subsurface infrastructure provided by Vandcenter Syd A/S (2019b) and the Danish Geodata Agency (2019).

https://doi.org/10.5194/hess-2022-330
Preprint. Discussion started: 4 October 2022

Figure 1b shows the imperviousness of the land cover and the location of infrastructure and basements. Approximately 50 % of the total land cover in the model domain is impermeable or semi-permeable such as buildings, asphalt, and concrete pavement, which have an imperviousness above 75 %. This high percentage of imperviousness is dominant in the northern and eastern parts of the domain, see Figure 1b. The remaining land cover is unpaved, consisting of private and public green areas, minor deciduous forests, small ponds, and the two creeks. The distribution of the different land covers and the degree of imperviousness represent a typical urban area for larger Danish cities (population >100,000).

The length of the sewer pipe system within the model domain is 125 km and the majority of the pipes were established between 1960-1990 (Vandcenter Syd A/S, 2019b). The sewer system collects both stormwater runoff and wastewater; only in a few places in Odense, the two are separated. The drainage water generated in areas with separated systems is routed to the local rivers (Odense Kommune, 2011).

The local average precipitation is 761 mm year^{-1}, with a minimum of 41 mm in May and maximum of 81 mm in October. The average reference evapotranspiration is 629 mm year^{-1}. The highest temperatures are in August with a daily average of 17.2 °C and the lowest in January with a daily average of 1.7 °C (DMI, 2021). Since evapotranspiration is low in the winter period (October-March), most of the groundwater recharge occurs in this period.

The landscape is a low-lying moraine landscape shaped by glaciations; in the northeastern part of the model domain, the landscape changes into a late-glacial plain (Mielby and Sandersen, 2017; Jakobsen and Tougaard, 2018). The predominant Quaternary deposits consist of glacial clay till - a mixture dominated by clay with contents of sand, gravel, and stones - and diluvial sand and clay deposited by glacial meltwater. The Quaternary deposits reach down to approximately -50 m.a.s.l. and locally even below -100 m.a.s.l., as seen in Figure 2.

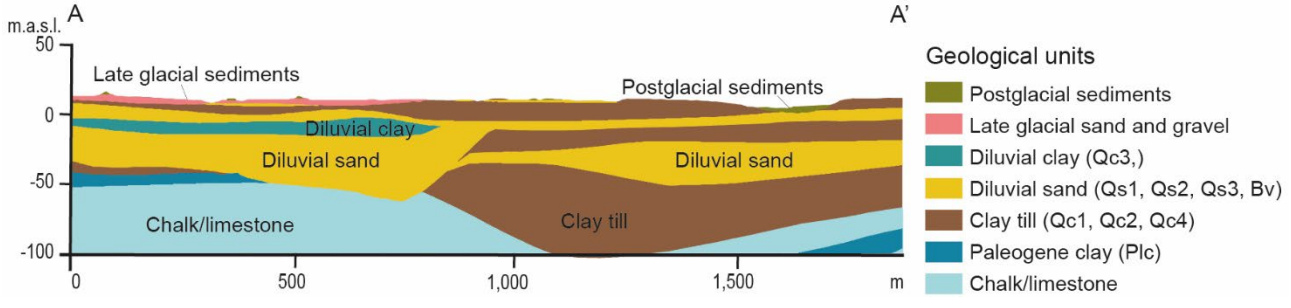

Figure 2. Geological cross-section of profile A-A'. See Figure 1 for the location of the profile.

At the terrain, the moraine landscape is dominated by clay till, while the late glacial plain is dominated by late-glacial sand and gravel, transported by meltwater from the last ice sheet (Weichselian). In the low-lying areas along the streams, postglacial deposits such as peat or gyttja dominate the shallow geology (Sandersen and Kallesøe, 2017; Jakobsen et al., 2022). In the urban area, the material composition of the first 1-5 meters can vary within short distances depending on anthropogenic activity. Both the shallow and deeper subsurface beneath the city are less well documented, compared to the open land area. Below the Quaternary deposits follows a layer of impermeable Paleogene clay, which is overlaying Danian limestone and Cretaceous chalk (Sandersen and Kallesøe, 2017).

https://doi.org/10.5194/hess-2022-330
Preprint. Discussion started: 4 October 2022


Hydrology and Earth System Sciences
Discussions

The oldest Quaternary layers have locally been eroded by subglacial meltwater streams, which created buried valleys that in some areas reach down into the Paleocene clay and the limestone/chalk beneath (Sandersen and Jørgensen, 2016). Two buried valleys have been documented west and southeast of Odense City center. The oldest valley has a NE-SW orientation and the younger buried valley has an E-W orientation. Previous studies indicate that the two valleys unite just outside the Bolbro district, see Figure 1, with a younger regional sand layer and it has been suggested that the E-W oriented valley continues east beneath the City of Odense (Sandersen and Kallesøe, 2017). The sandy infill of the two buried valleys and an overlaying regional sand layer are the primary aquifers used for water abstraction in Odense. The local sand and gravel deposits of the late glacial plains and anthropogenic fill material form secondary shallow aquifers (Vandcenter Syd A/S, 2021). The shallow groundwater in the city of Odense threatens buildings and infrastructure when groundwater levels are high which typically occurs in late winter and early spring. Since 2006 approximately 1-2 mill. m^3 $year^{-1}$ is pumped from five abstraction wells for the local water supply. These are located in the center of the model domain, outside the city center, see Figure 1. The wells abstract water from the buried valleys and the regional sand layer.

3 Materials and methods

The effect of the geological configuration was analyzed by applying three geological models V0, V1, and V2 in otherwise identical integrated hydrological models. The effect of computational grid size on the hydrological simulations was examined by using two different horizontal grid sizes in the hydrological model, respectively 50 m and 10 m resolution. Post calibration the effect of the geological configuration and grid size was analyzed based on their simulation of high-water levels, the 95th percentile, and particle tracking.

3.1 Geological models

The geological model V0 was an existing hydrostratigraphical layer model developed for the larger Odense City area by Sandersen and Kallesøe (2017). The geological models V1 and V2 were developed as part of this study. The V0 model represents the Quaternary deposits and the pre-quaternary deposits of Paleogene clay and limestone/chalk down to -150 m.a.s.l. The interpretation of the upper geological layers did not include data on fill and anthropogenic materials. The geological models V1 and V2 represent the shallow urban geology down to 15 m below the terrain, in voxels, while below 15 m depth the models retained the deeper stratigraphical layers from V0.

The method used for modeling the shallow urban geology in V1 and V2 follows the procedure presented by Mielby and Sandersen (2017). The method involves the following steps: (1) convert the upper layers of the hydrostratigraphical model corresponding to the extent of the anthropogenic layer to voxels for a designated spatial discretization, and (2) assign a sand/clay fraction to each voxel corresponding to the materials' lithology, (3) implement anthropogenic data such as basements, pipelines and utility trenches in the voxel model and assign a categorical value to each data type, (4) compute

https://doi.org/10.5194/hess-2022-330
Preprint. Discussion started: 4 October 2022


Hydrology and Earth System Sciences
Discussions

representative voxel values according to volume when several anthropogenic data occur in the same voxel, and (5) merge the voxel model of the shallow urban geology with the hydrostratigraphical model of the deeper geological sediments.

The voxel models for V1 and V2 were constructed with a grid size of 5x5x1 m using a 3D floating-point grid in the geological modeling software GeoScene3D (www.i-gis.dk). The vertical extent of the voxel models was from the terrain to 10 meters below the lowest elevation point. The defined grid size was a trade-off between being able to represent the anthropogenic structures in the uppermost subsurface and computational constraints.

In model V1, data on urban subsurface infrastructure; utility trenches, pipes, roads and roadbed, railway tracks, basements and foundation materials were incorporated, based on the model procedure described above. The V2 voxel model included the same data on urban infrastructure as in V1 and additional data on soil material in the top 5 meters. The different data and sources utilized for the geological models are presented in supplementary material (Table S1). The modeling procedure for the V2 model of the shallow geology started with the input from V0, followed by overwriting the upper first meter with soil data and modeling the fill layers based on descriptions from shallow geotechnical boreholes. A zone around the boreholes with a radius of 12 m was applied, where the fill material was assumed to be present. Finally, the anthropogenic infrastructure data also used in V1 was added.

The sand/clay fractions in the voxels represent the expected content of sand and clay in the lithology of the geological layer or the equivalent properties for the subsurface infrastructure. The fraction values vary between 0 and 1 corresponding to 100 % clay and 100 % sand, respectively.

Table 1. Sand/clay fractions for the different geological units and infrastructures used in the voxel models

Geological unit	Sand/clay fraction
Postglacial sediments	0.5
Peat	0.5
Gyttja	0.3
Sand and gravel from late-glacial	1
Clay from late-glacial, glacial lakes	0
Freshwater clay, saltwater clay	0.8
Freshwater sand, saltwater sand	0.8
Diluvial silt	0.4
Diluvial clay (Qc)	0
Diluvial sand, diluvial gravel (Qs)	1
Clay till (Qc)	0.7
Infrastructure unit	**Sand/clay fraction**
Trenches (mains and other pipelines)	1
Roads (Base/embankments)	1
Railroads (Base)	1
Basements and fundaments	0
Fill	1

Assumptions of the sand/clay fractions were necessary since the description of the fill materials is often poor and often refers to standards. The type of infill material used in construction depends on age as well as the type of the infrastructure

https://doi.org/10.5194/hess-2022-330
Preprint. Discussion started: 4 October 2022

Hydrology and Earth System Sciences
Discussions

(Kristensen et al., 2015). The characteristics of the infill materials have not been recorded and the infill may change over very short distances even for structures from the same period. The sand/clay fractions for the infrastructure classes, in Table 1, thus represent very diverse and inhomogeneous infills.

Each voxel was assigned a representative sand/clay fraction based on volume averaging of the sand/clay fractions representing the lithologies and the infrastructures occurring in the voxel, see Figure 3.

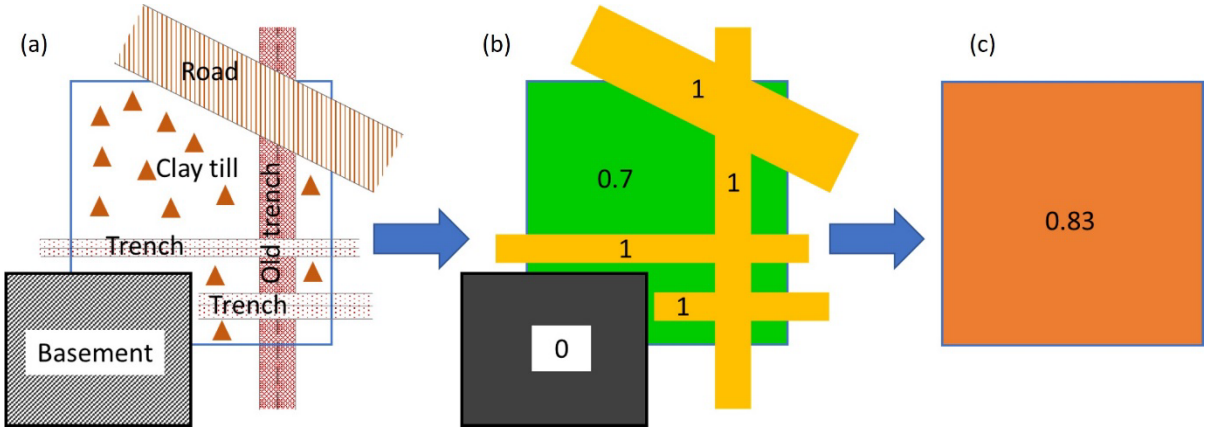

Figure 3. Workflow for setting the value of a voxel: (a) Voxel with clay till and anthropogenic subsurface structures, (b) The corresponding sand/clay fractions, and (c) the resulting representative sand/clay fraction for the voxel, which is based on average according to volume.

When defining the infrastructure settings, the locations of roads or pipes available as GIS overlays were used as proxies for the presence of excavations and trenches. Data of infill materials and characteristics were estimated from borehole data in combination with information on age and knowledge of past and current standards for the size of trenches and the fill material in the excavations (Mielby and Sandersen, 2017). Data on subsurface electrical installations and other minor service lines were not considered as their spatial extent was negligible in relation to the chosen model resolution.

3.2 Hydrological models

3.2.1 Model components

The integrated hydrological model was based on the MIKE SHE code (Abbott et al., 1986 a,b). The model components applied for the MIKE SHE setup were: (1) Overland flow, described by a finite difference approximation to the 2D Saint Venant equations for diffusive flow. Overland flow is generated when precipitation is higher than the infiltration capacity due to either high groundwater levels or ponding at the surface. Reduced infiltration capacity was specified in paved areas, and drainage of ponded water was specified by the imperviousness of the land cover. (2) Unsaturated flow, described by a simplified two-layer water balance approach assuming vertical flow and a conceptual formulation for actual evapotranspiration. This approach is primarily applicable to areas where the groundwater table is shallow and the actual

https://doi.org/10.5194/hess-2022-330
Preprint. Discussion started: 4 October 2022


Hydrology and Earth System Sciences
Discussions

evaporation rate is close to the potential rate (Butts and Graham, 2005), which is the case for the study site. (3) Saturated flow, described by the governing equation for 3D saturated flow based on Darcy's law. Subsurface drainage is included as a sink term in the equation and depends on the groundwater level, depth of the drain, and a time constant. Detailed descriptions of the components can be found in DHI (2020).

The three hydrologic components were run with independent time steps and automatically controlled to secure accurate water balances. The maximum time steps for the three components were: 0.5 hours for overland flow, 6 hours for unsaturated flow, and 12 hours for groundwater flow. MIKE SHE was coupled to MIKE HYDRO (DHI, 2017) for the simulation of stream flow in the two creeks in the model domain. The kinematic wave approximation was used with a fixed time step of 10 minutes.

3.2.2 Model input and parameterization

The model was driven by daily values of precipitation, temperature, and reference evapotranspiration, which were retrieved as daily averaged gridded data (10 x 10 km) from the Danish Metrological institute (DMI, 2021).

A digital terrain model (DTM) in 10 m resolution (Danish National Agency for Data Supply and Infrastructure, 2019) was used as the surface elevation of the hydrological models, and a land-use map in 10 m raster resolution from Levin et al. (2017) was used as a basis for the vegetation characterization in the model. The land-use map contains 36 land use classes, these were reclassified into 6 classes: buildings, grass, deciduous forest, coniferous forest, agriculture, and water bodies. Buildings and grass are the dominant classes in the domain. For each land-use class, a monthly variation of leaf area index and root depth was defined. The initial parameter values were retrieved from the National hydrological model of Denmark (DK-model) (Stisen et al., 2019).

Data on imperviousness was derived from land cover data (Levin et al., 2012) in 10 x 10m resolution and combined with the local water supply's map of imperviousness (Vandcenter Syd A/S, 2019a). The latter map was used to exclude the areas with no overland drainage. In the resulting imperviousness map, the data were grouped in quartiles and used to estimate the paved area fraction for each grid cell, see Figure 1a. The paved area fraction was used to define the overland drain runoff coefficient of ponded water and the classification of detention storage. Moreover, it was used as a linear scaling fraction for the surface-subsurface leakage coefficient, which reduces infiltration in paved areas. This is referred to as the effective leakage coefficient (DHI, 2020). The surface-subsurface leakage coefficient was given the value $6x10^{-7}$ s^{-1} in all cells. Surface-subsurface leakage was considered for areas with a paved area fraction larger than 0.5

Overland flow occurs when the detention storage capacity is exceeded representing the depth of water retained in local depressions due to heterogeneities/roughness of the land surface. The detention storage was set to 1 mm for cells with a paved area fraction ≥ 0.75 assuming a very smooth surface, while the remaining grid cells were given a value of 4 mm. Overland flow is controlled by the surface roughness described by the Manning M which was set to 10 $m^{1/3} * s^{-1}$ for the entire domain.

https://doi.org/10.5194/hess-2022-330
Preprint. Discussion started: 4 October 2022


Hydrology and Earth System Sciences
Discussions

Drainage of overland water was assumed to occur from paved road networks and larger sealed surfaces. Cells with a paved area fraction larger than 0.5 were considered to be part of the overland drainage network, whereas cells with a lower value were assumed to be green areas and not attached to the overland drainage system. The time constant for the overland drains was set to 0.001 s^{-1}. This is a relatively high leakage coefficient, which in most cases will drain all available ponded water from the cell.

The three geological models, V0-V2, were tested in the otherwise identical hydrological models. The subsurface component of the hydrological model had 14 computational layers. The thickness of the computational layers and their outer boundary conditions is specified in **Fejl! Henvisningskilde ikke fundet.**, and even though the geological models were altered the computational layer settings were kept constant. The hydraulic properties of the subsurface system were assigned to the geological units within the computational layers. This made it possible to assign individual parameter values to the stratigraphic layers, lenses, and the sand/clay fraction classes in the V1 and V2 models.

The boundaries of the model domain follow natural boundaries in the upper 8 meters of the model. The boundary conditions for the conductive layers below 8 meters were specified using a nested modeling approach, where a regional model (Kidmose and Sonnenborg, 2018) was used to calculate head boundary conditions for this city-scale domain, Table 2.

Table 2: Conditions for the computational layers in the hydrological models

Computational layer no.	Layer thickness (m.b.g.l.)	Hydrogeology in the V0 model (abbreviation for the hydrostratigraphical layer)	Outer boundary condition*
1	0-1	Postglacial soils, late glacial sand, and gravel	Zero flux
2	1-2		Zero flux
3	2-4		Zero flux
4	4-6		Zero flux
5	6-8	Clay till (Qc1)	Zero flux
6	8-10	Diluvial sand and gravel (Qs1)	Specified head
7	Distributed	Clay till (Qc2)	Zero flux
8	Distributed	Diluvial sand and gravel (Qs2)	Specified head
9	Distributed	Diluvial clay (Qc3)	Zero flux
10	Distributed	Diluvial sand and gravel (bv)	Specified head
11	Distributed	Clay till (Qc4)	Zero flux
12	Distributed	Diluvial sand and gravel (Qs3)	Specified head
13	Distributed	Paleogene clay (Plc)	Zero flux
14	Distributed	Limestone/Chalk	Specified head

*A zero flow condition was assumed for all layers along the eastern boundary of the domain since this part follows the Odense River.

Since the objective was to analyze the impact of the shallow urban geology, the vertical resolution of the computational layers was set to 1 meter at the top and increases with depth until layer six, 10 m below the terrain. From layer seven and

https://doi.org/10.5194/hess-2022-330
Preprint. Discussion started: 4 October 2022


Hydrology and Earth System Sciences
Discussions

down, the computational layer thickness follows the extent of regional layers from the regional model. The small layer thickness at the top of the model was specified to resolve the variation of the anthropogenic geology in the geological models V1 and V2. The layer thickness was set to increase with depth because the anthropogenic effect is expected to decrease with depth and a coarser computational grid reduces the computational burden.

Saturated zone drainage was represented in the models at distributed depths based on three assumptions: (1) the sewer system in the impervious part of the urban model was leaky and the sewer pipes act as saturated zone drains if the groundwater level reaches the level of a sewer pipe, (2) buildings with basements all have perimeter drains installed at 3 m b.g.l. (below ground level) except for basements at two locations, where the basement reaches down to respectively 4 and 10 m b.g.l., and (3) in green and forested areas as well as open landscapes drain depth was assumed to be 1 m b.g.l.

The location and depth of the sewer system were provided by the local wastewater company (Vandcenter Syd A/S, 2019b) and data on buildings with basements were received from the municipality (Odense Kommune, 2019). In the model setup, the drainage of groundwater into the sewers and the drains was assumed to be the same for the entire domain. The water collected by the drains is discharged to either one of the two streams in the model, or out of the model if the area is not a part of a contributing area to the streams.

3.3 Calibration

The hydrological models were calibrated using the parameter estimation tool PEST (Doherty, 2016b, a) following the same procedure for all 6 models. In the calibration scenarios, the model was run for the period 2012-2020, where 2012-2014 was used as a warm-up and 2015-2020 as the calibration period.

Time series of observations of the hydraulic head from 50 wells and stream discharge from one station were used for calibration. The local water supply company Vandcenter Syd A/S (2021) provided 16 hydraulic head time series from both shallow and deep aquifers, which covered the entire calibration period, while the remaining 14 time series were from shallow wells that were established in 2019 as part of this study and therefore these time series only covers the year 2020 of the calibration. The discharge time series covers the entire calibration period and was derived from a Q/h rating curve of stream measurements undertaken in 2019 and 2020 from the Hedebækken river as part of this study. The location of the observation wells and stream gauge is shown in Figure 1. Several of the observation wells had 2-4 well screens for observation of deep and shallow aquifers. Half of the well screens were assumed to be placed in shallow aquifers due to their shallow depth and the lithological characterization from the boreholes.

The parameters selected for calibration (free parameters) and the ones tied to the calibration parameters were based on a sensitivity analysis, where all model parameters were analyzed.

The sensitivity analysis was based on composite sensitivities as described in Doherty (2015) was conducted for all 96 model parameters. Based on the analyses across all models a set of free parameters was selected subject to calibration and a set of parameters to be tied to the free parameters. One parameter set was selected for the V0 model sand one parameter set was selected for the V1 and V2 models, see Table 3.

https://doi.org/10.5194/hess-2022-330
Preprint. Discussion started: 4 October 2022

Hydrology and Earth System Sciences
Discussions

It was chosen to tie the vertical and horizontal conductivities and the sand/clay fraction classes to maintain their linear relationship with increasing sand content. One can argue that the sand/clay fraction was calibrated as one class. For parameters with little sensitivity and not subject to calibration their values were instead estimated from past model experiences.

Table 3. Parameter sets for calibration, h stands for horizontal, v stands for vertical, and the S10-S100 stands for the sand/clay fraction classes, where e.g., S100 is the sand/clay fraction 0.9-1.

Calibration parameter set for V0 models			Calibration parameter set for V1 and V2 models		
Description of free parameter	Abbreviation of free parameter	Tied parameter(s)	Description of free parameter	Abbreviation of free parameter	Tied parameter(s)
Horizontal hydraulic conductivity for Quaternary buried valley	$K_{bv2,h}$	$K_{bv2,v}$	Horizontal hydraulic conductivity for Quaternary buried valley	$K_{bv2,h}$	$K_{bv2,v}$
Horizontal hydraulic conductivity for Quaternary sand 2	$K_{Qs2,h}$	$K_{Qs2,v}$, $K_{Qs3,h}$, $K_{Qs3,v}$	Horizontal hydraulic conductivity for Quaternary sand 2	$K_{Qs2,h}$	$K_{Qs2,v}$, $K_{Qs3,h}$, ,$K_{Qs3,v}$
Vertical hydraulic conductivity for Quaternary clay	$K_{Qc,v}$	$K_{Qc,h}$	Vertical hydraulic conductivity for Quaternary clay	$K_{Qc,v}$	$K_{Qc,h}$, $K_{S20,h}$, $K_{S20,v}$ $K_{S30,h}$, $K_{S30,v}$ $K_{S40,h}$, $K_{S40,v}$
Saturated zone time constant	C_{riv}		Saturated zone time constant	C_{riv}	
Saturated zone time constant	C_{dr}		Saturated zone time constant	C_{dr}	
Root depth of permanent grass	$D_{r,grass}$	$D_{r,decid}$	Root depth of permanent grass	$D_{r,grass}$	$D_{r,decid}$
Leakage coefficient, Rivers	C_{riv}		Leakage coefficient, Rivers	C_{riv}	
Horizontal hydraulic conductivity for Clay till	$K_{ct,h}$	$K_{ct,v}$	Horizontal hydraulic conductivity for sand/clay fraction 0.6-0.7	$K_{S70,h}$	$K_{S100,h}$, $K_{S100,v}$ $K_{S90,h}$, $K_{S90,v}$ $K_{S80,h}$, $K_{S80,v}$ $K_{S70,v}$, $K_{S60,h}$, $K_{S60,v}$ $K_{S50,h}$, $K_{S50,v}$
Specific storage for Quaternary buried valley	$S_{s,bv2}$				

For calibration, Tikhonov regularization based on preferred values in combination with Singular Value Decomposition (SVD) was used (Doherty, 2015). To account for regularization a Tikhonov regularization term was included in the objective

https://doi.org/10.5194/hess-2022-330
Preprint. Discussion started: 4 October 2022


Hydrology and Earth System Sciences
Discussions

function, which was minimized as a compromise between minimizing the measurement objective function and the regularization term representing the deviation from the initially preferred parameter values (Doherty, 2015). The total objective function, Φ_t, is given in Ep. (1).

$$\Phi_t = \Phi_m + \mu^2 \Phi_r \quad (1)$$

where Φ_m is the measurement objective function given by Eq. 3.2, Φ_r is the regularization objective function and μ^2 is the global regularization weight factor.

The measurement objective function was defined as the sum of squared weighted residuals of hydraulic heads (h), head amplitude (ampl), and stream discharge (d):

$$\Phi_m = \alpha_h * \sum_{i=1}^{h}(\omega_{hi}(h_{obs,i} - h_{sim,i}))^2 + \alpha_{ampl} * \sum_{j=1}^{ampl}(\omega_{dj}(ampl_{obs,j} - ampl_{sim,j}))^2 + \alpha_d * \sum_{k=1}^{d}(\omega_{hk}(d_{obs,k} - d_{sim,k}))^2 \quad (2)$$

where α is the group weight, ω is the weight of the observations. For optimizing the parameters, more weight was given to hydraulic head observations than to discharge observation data. The following group weights were assigned in the objective function Eq. (2): head (0.45), head amplitude (0.45), and discharge (0.10).

The regularization objective function was defined by

$$\Phi_r = \sum_{i=1}^{p}(\mu_{p,i}{}^2(p_{ini,i} - p_{adj,i}))^2 \quad (3)$$

where p is the parameter-set, $p_{ini,i}$ is the preferred value for parameter i, $p_{adj,i}$ is the estimated value for parameter i, and $\mu_{p,i}{}^2$ is the differential regularization weight factor (Doherty, 2015).

The regularization weight factor μ^2 was constrained by a target measurement objective function Φ_m^t, which implies that the model is considered calibrated when the measurement objective function is equal to or below Φ_m^t. In addition, an acceptable measurement objective function Φ_m^a is defined below which the calibration is accepted.

The selection of appropriate target and acceptable measurement objective functions Φ_m^t and Φ_m^a is subjective and must be assessed during the calibration process (Doherty, 2015). The target and acceptable objective measurement function were defined by first running the optimization without regularization and then subsequently specifying Φ_m^t to 5-10% higher than the objective function obtained from the initial run. The acceptable measurement objective function Φ_m^a was specified 5% higher than the target measurement objective Φ_m^t as suggested by Doherty (2015). An overview of the hydrological models, their differences in geology and computational grid size, and the calibration setup can be found in the supplementary material (Table S2).

The goodness of fit for the calibrated models was assessed based on the average error statistics and the spatial distribution of the mean error (ME) of simulated heads. The parameter uncertainty was estimated based on linear statistics and using the measures of parameter identifiability, comparison of estimated parameters and prediction uncertainty as suggested by Doherty (2016b).

https://doi.org/10.5194/hess-2022-330
Preprint. Discussion started: 4 October 2022


Hydrology and Earth System Sciences
Discussions

3.4 Particle tracking

Particle simulations were carried out for all the calibrated models to compare the distributions of travel time and the distribution of the particles at end sinks across the different model versions. Forward particle tracking was based on interpolated velocity fields.

The particle tracking was carried out for 200 years looping the dynamic flow fields for the calibration period 2015-2020. Particles were released at the initial timestep uniformly in each cell from layers 1-6. They were thus released throughout the anthropogenic model layers from terrain and down to 10 m.b.g.l. To be consistent and have a comparable number of particles across models with different grid sizes, only one particle was released in each cell in the 10 m models, while 25 particles were released in each cell in the 50 m models. A total of 625,300 particles were released in the 50 m models and 595,618 in the 10 m models. If particles are released above the water table, they are immobilized and will not be part of the analysis.

4 Results

4.1. Geological models

The A-A' cross-section from the initial stratigraphical model, V0, a voxel model of V0, and the two urban voxel models V1 and V2 are shown in Figure 4. The V0 voxel model was used as a step before the infrastructure data was added and converted to model V1, but the V0 voxel model was not used in the hydrological model. Yet, it was decided to compare the V0 voxel model with the V1 and V2 voxel models to make a quantitative comparison between the models, see Figure 5. The differences between the models mainly occur in the uppermost 1-3 m.b.g.l. where most of the anthropogenic structures primarily are located. From Figure 5, notably, models V1 and V2 have more sand/clay fraction classes embedded as opposed to the voxel model V0 where only 4 classes are present.

Overall, the V2 voxel model is not very different from the V1 voxel model. In the V2 model, the sandy material became more sandy and the low permeable material became less permeable, see Figure 4c-d. The geological structures deeper than 5 m below the surface remained the same in all three models, except at a few locations where additional data suggested that a basement under a hospital extended deeper. Therefore, the two dominant voxel classes in the deeper layers, the sand/clay fractions 0.6-0.7 and 0.9-1.0, have approximately the same relative volume in all three models, 37% and 56%, respectively. Thus, the difference between models is only apparent in the remaining 7% of the total volume.

https://doi.org/10.5194/hess-2022-330
Preprint. Discussion started: 4 October 2022

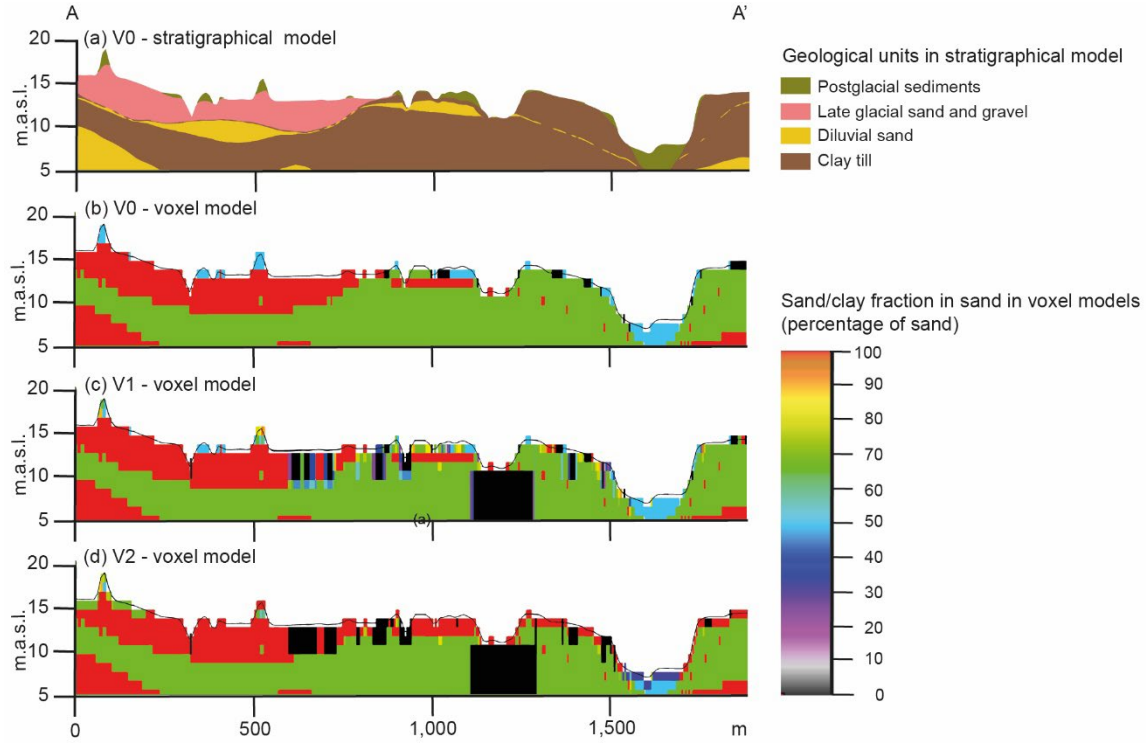

Figure 4. Profile A-A' from the geological models V0 – stratigraphical model (a), V0 – voxel model, (b) V1 – voxel model (c) and V2 – voxel model (d).

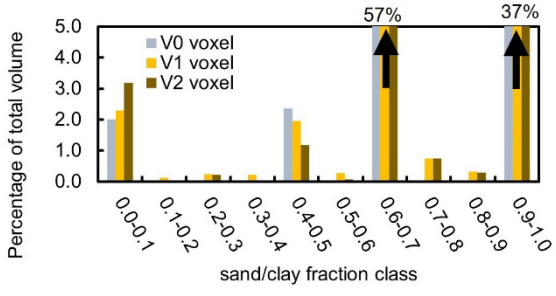

Figure 5. Percentage of the sand/clay fractions of the total volume of the geological voxel models V0, V1, and V2. Note that the sand/clay fractions 0.6-0.7 and 0.9-1.0, respectively take up about 37 % and 56 % in all models, and plot beyond the range of the y-axis.

The largest differences between the relative volumes of the voxel fractions are seen for the two classes 0.0-0.1 and 0.4-0.5. The relative volume of the most impermeable fraction class 0-0.1 increased slightly as the infrastructure data was added in V1, while it increased more than one-third between V0 and V2. On the contrary, the relative volume of fraction class 0.4-0.5 decreased as data on infrastructure and near-terrain geology were added in V1 and V2.

https://doi.org/10.5194/hess-2022-330
Preprint. Discussion started: 4 October 2022

Hydrology and Earth System Sciences
Discussions

4.2 Calibration of hydrological models

Figure 6 depicts the three error statistics, i.e. the root-mean-square error of heads (RMSE_h) and stream discharge (RMSE_Q) and residual of yearly groundwater head amplitude (ErrAmpl_h). The error statistics indicate an overall good performance for all models and a similar level of fit to the head and discharge observations. Nevertheless, RMSE_h for the V1_10 and V2_10 models was 20 cm lower compared to the other models while ErrAmpl_h was about the same and RMSE_Q slightly higher.

Analyzing RMSE_h of the shallow and deep well screens individually, RMSE_h was 1.0 m for the shallow well screens in the urban models and 1.2 m for the shallow well screens in the V0 models. On the other hand, RMSE_h was 1.7-1.8 m for the deep wells in the urban models, and 1.6 m and 1.8 m for the two models V0_50 and V0_10, respectively.

ErrAmpl_h varied between 0.2 m and 0.3 m across the different model versions. For V0_10 and V0_50 ErrAmpl_h was 0.2 m, while for all the V1 and V2 models the ErrAmpl_h was 0.3 m, Figure 6. This appears as a reasonable accuracy since most of the head time series have an annual amplitude of 0.5-1.0 m.

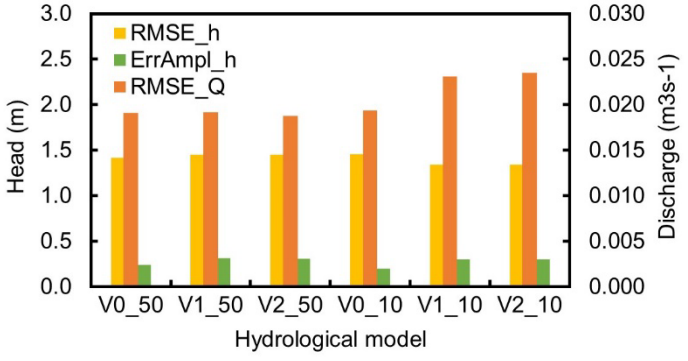

Figure 6. A plot of simulated error statistics based on three metrics, i.e., root-mean-squared-error (RMSE) of heads (h), RMSE of discharge (Q), and error of yearly groundwater head amplitude (ErrAmpl_h).

RMSE_Q was 0.019 m^3s^{-1} for all models in 50 m resolution and V0_10, while V1_10 and V2_10 have slightly higher RMSE_Q values, see Figure 6. The calibration was found to be acceptable since the average discharge observation is 0.08 m^3s^{-1}, and the accuracy of the measurements is small because of an uncertain rating curve. Furthermore, discharge was only weighted by 10% in the objective function.

As an example of the model accuracy, Figure 7 shows the simulated and observed hydraulic heads for the six models for one of the shallow observation wells.

https://doi.org/10.5194/hess-2022-330
Preprint. Discussion started: 4 October 2022

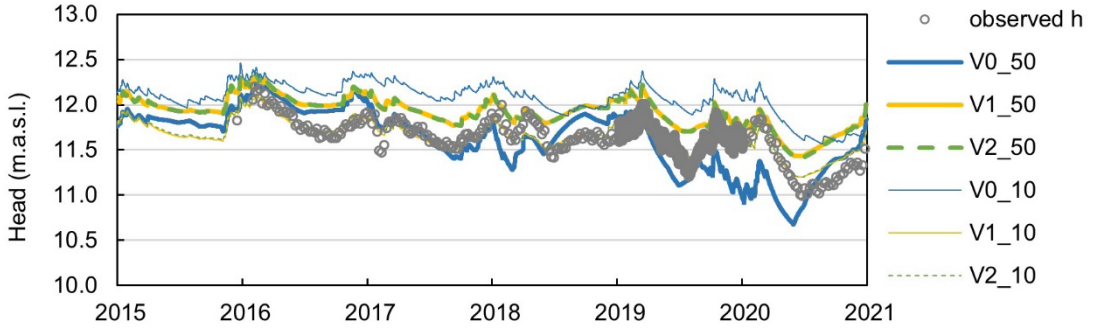

Figure 7. Observed and simulated head for a shallow well screen (145.2424_3, see Figure 1)

The spatial distribution of mean error (ME) for simulated heads is depicted in Figure 8 and generally shows similar tendencies. The ME is within +/- 1 m for most of the shallow well screens with a few outliers, and within +1 to -2 m for the deep screens. The best fit to the simulated heads was obtained in the central part of the model area. However, here more observation wells are available with time series that cover the whole calibration period. All models underestimate (orange and red colors) the groundwater level in the north-western part of the model area, while most of the models also have issues with underestimated groundwater levels close to the boundary in the southeastern part of the model area. The underestimation in the north-western part may be related to perched water tables not considered in the models and because of the scarcity of wells in this area.

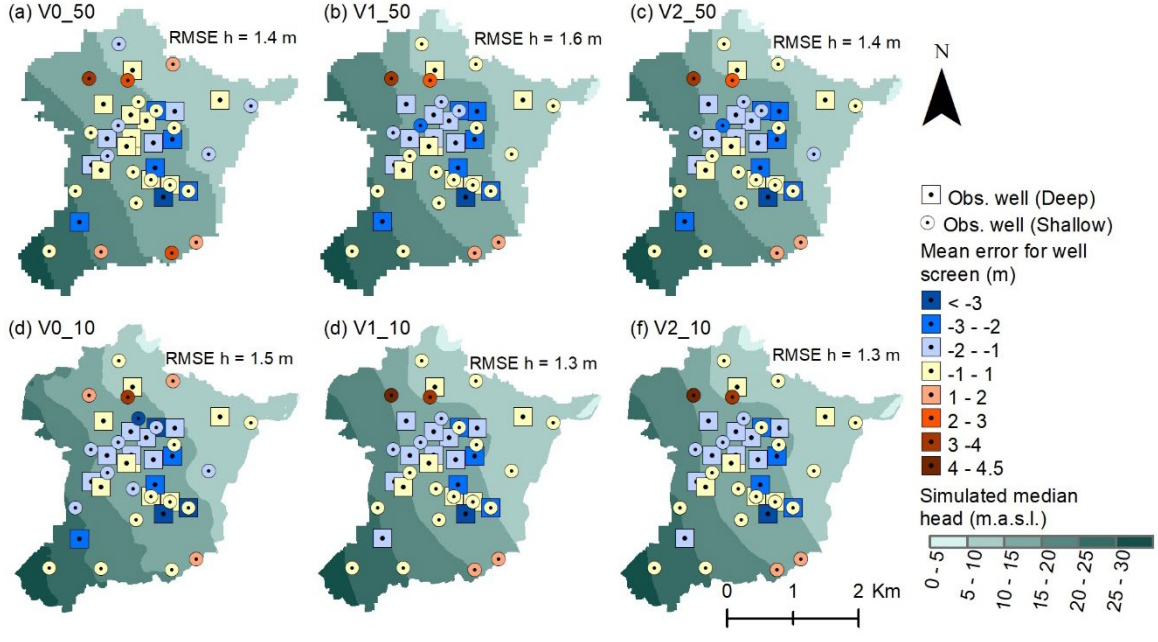

Figure 8. Mean error of simulated hydraulic head, where the circle signature represents the shallow well screens and the square signature represents the deep well screens. The background map shows the median simulated head.

https://doi.org/10.5194/hess-2022-330
Preprint. Discussion started: 4 October 2022

Hydrology and Earth System Sciences
Discussions

The calibration setup ensured that the models achieved a measurement objective function Φ_m within the range of the target Φ_m^t and acceptableΦ_m^a objective function. Figure 9 shows the preferred initial parameter values (- symbols) together with the estimated parameter values with regularization (o-symbols) and without (x-symbols). Many of the parameter estimates are different from their initial values when the models were calibrated without regularization while the regularization as expected made some of the parameters come closer to the preferred values. When regularization was used, the parameters of hydraulic conductivities $K_{j25,h}$, $K_{qs2,h}$, and $K_{qc,v}$ in the V0_50 model show the largest difference from the initial parameters. In contrast, all parameter values estimated in the V0_10 model were close to the initial values. For V0_50 only, the discrepancy between the estimated vertical hydraulic conductivity of quaternary clay $K_{qc,v}$ and the initial value was larger when the models were calibrated with regularization.

The parameter estimates of the V1 and V2 models are generally close to the initial parameter values, see Figure 9. When regularization was included the largest deviation from the initial values occurred for the hydraulic conductivity of the two sandy materials $K_{qbv2,h,}$ and $K_{s70,h}$, with a factor of 0.8 and 0.6, respectively.

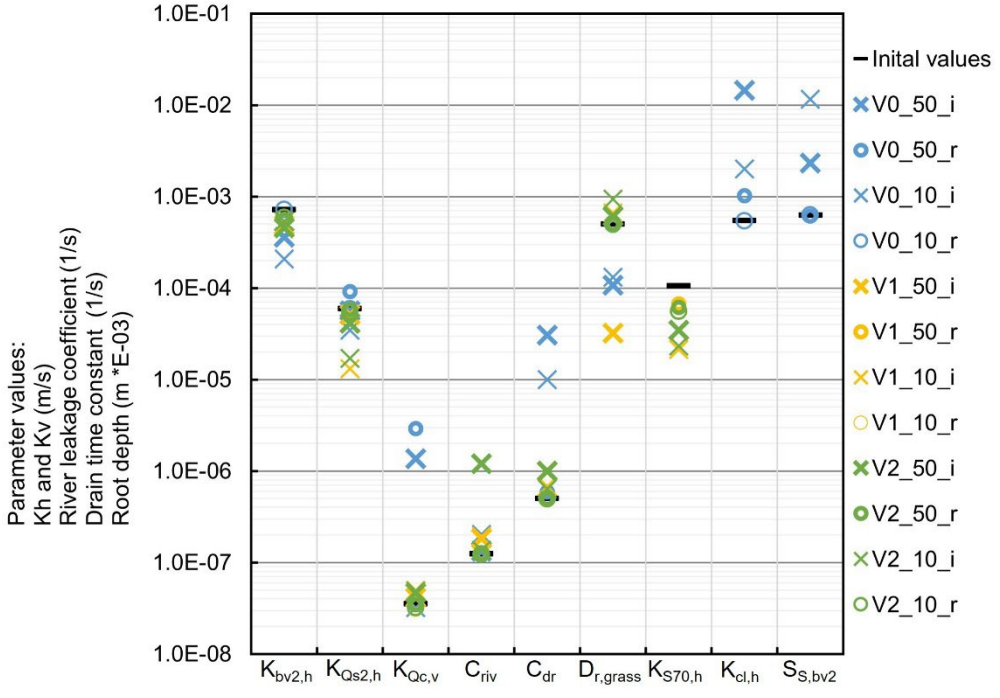

Figure 9. Initial preferred parameter values and estimated values of free parameters for models calibrated without regularization (i) (x-symbol) and models calibrated with regularization (r) (o-symbol).

The bar charts in Figure 10 illustrate the contribution of the singular values to the identifiability and indicate which parameters' relative error variance can be reduced by calibration (Doherty, 2015). Since the parameters' identifiability was not truncated all parameters have a value of one.

https://doi.org/10.5194/hess-2022-330
Preprint. Discussion started: 4 October 2022

Hydrology and Earth System Sciences
Discussions

Red-yellow colors indicate that the parameter is informed by observation data and that the parameter value's relative error variance can be reduced through calibration. Blue-green colors, on the other hand, indicate that the parameter estimation is less informed by the observation data and hence the relative error variance cannot be reduced by calibration (Doherty, 2015).

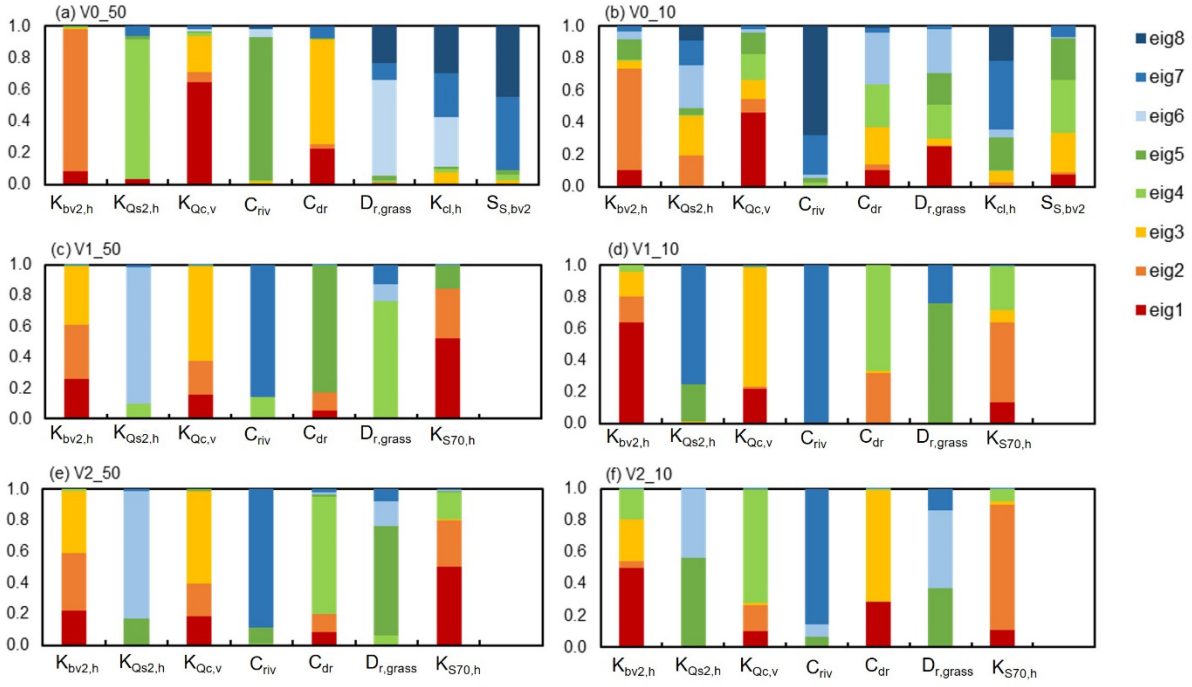

Figure 10. Parameter identifiability without truncation of the solution space. The colors indicate the contribution made to the total identifiability by different eigen vectors in the solution space.

Figure 10a-b depicts the parameter identifiability for the models V0_50 and V0_10 and show that the hydraulic conductivities $K_{qbv2,h}$ and $K_{qc,v}$ are well informed by measurements since they are dominated by red-yellow colors. For V0_50 the parameters dominated by blue-green colors are $K_{j25,h}$ and $d_{r,grass}$, while for V0_10 it is $K_{j25,h}$ and C_{riv}. For the V1 and V2 models the parameters $K_{qbv2,h}$, $K_{s70,h}$, and $K_{qc,v}$ are mostly dominated by red-yellow colors, while $K_{qs2,h}$, C_{riv}, and $d_{r,grass}$ are dominated by blue colors. Furthermore, for both models, the proportion of red color increases for Kqbv2,h when the model is run in 10 m resolution compared to the 50 m resolution. On the contrary, the proportion of red color decreases for parameter Ks70,h, when the model is in 10 m resolution compared to 50 m resolution.

The parameter values that deviate most from their preferred values are those that are dominated by red and orange colors in Figure 10 while parameters with more blue-green and more mixed color patterns obtain parameter values closer to their preferred value. This illustrates that the parameters which were less informed by the observations and less subject to a reduction in error variance by calibration are the ones dominated by blue to green colors. The parameter values obtained by the regularized inversion were considered realistic and well-defined and were accepted for further analysis.4.3 Simulation of high-water levels.

https://doi.org/10.5194/hess-2022-330
Preprint. Discussion started: 4 October 2022

Hydrology and Earth System Sciences
Discussions

4.3 Simulation of high-water levels

The 95th percentile of the simulated water table depths for all six models is shown in Figure 11. All panels in Figure 11 show the same general pattern. 0-2 m water table depth in the lowlands and along the rivers, and above 10 m depth in the northwestern part and south part of the model domain. The 50 m models resulted in very similar results in Figure 11a-c, especially the models V1_50 and V2_5. Yet, the models V1_50 and V2_50 resulted in a slightly less depth to the water table in the areas with high imperviousness in the north and the center of the model domain, than the model V0_50.

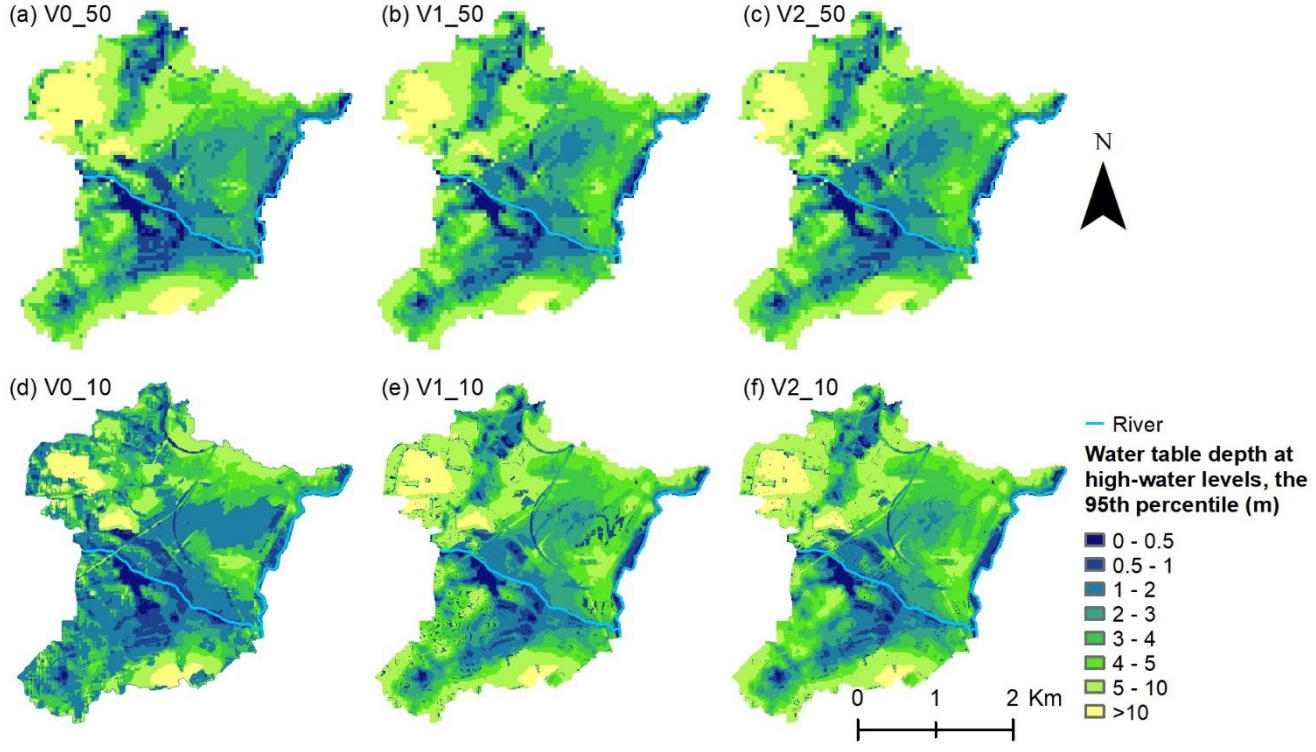

Figure 11. The 95th percentile of the simulated water table depth

The high-water simulation from the 10 m models V1_10 and V2_10 again showed very similar results, see Figure 11 d-f, with a small deviation from the 50 m models, yet the finer resolution allowed for more local variation. Meanwhile, the model V0_10m showed the largest area with the water table depth ranging from 0-2 m, see Figure 11d.

4.4 Particle tracking

In Table 4, the average, median, and 5th and 95th percentiles of travel times for particles reaching a sink are listed. Note that some particles were captured in the unsaturated zone and not tracked in the subsurface and as such represents one sink type. Other sinks include drainage to stream, drainage to the model boundary, and baseflow to rivers.

https://doi.org/10.5194/hess-2022-330
Preprint. Discussion started: 4 October 2022


Hydrology and Earth System Sciences
Discussions

Table 4. Statistics on simulated particle tracking for particles reaching sinks.

	Average travel time (yrs)	Median travel time (yrs)	5th percentile of travel time (yrs) [days]	95th percentile of travel time (yrs)	Percentage of released particles registered in layer 8 (regional sand aquifer) (%)
V0_10m	37.2	8.6	0.06 [21]	158	25
V1_10m	7.3	2.4	0.06 [22]	24	8
V2_10m	7.0	2.4	0.07 [25]	21	9
V0_50m	37.0	22.7	0.10 [35]	133	34
V1_50m	17.7	4.5	0.08 [31]	106	12
V2_50m	17.6	4.6	0.09 [33]	103	13

Tracking of particles to sinks resulted in a right-skewed distribution, with 5-10% of particles reaching a sink within 0.25 years and 25-60 % of the particles reaching a sink within 10 years depending on the model version. The 10 m models resulted in a smaller median travel time than the corresponding 50 m models and the urban models V1 and V2 had a smaller median travel time to sink than in the V0 models for both 10 m and 50 m resolutions. The average travel time for V0_10 and V0_50 were both 37 years while the median was estimated to be 22.7 years and 8.6 years, respectively. This indicates that the travel time distribution for V1_10 is more skewed towards longer travel times than the V0_50 model.

The number of particles reaching the deeper groundwater is much higher for models V0_10 and V0_50 than in the other models which had urban geology represented, see Table 4.

Figure 12 depicts the release location of particles that represent the 5th percentile of travel times to sinks. Again, the largest differences are seen between the V0 models and the two urban models V1 and V2. When the models are run in 50 m resolution the locations of the V1 and V2 overlap (Figure 12b-c) while for 10 m resolution the release locations show some differences (Figure 12e-f).

https://doi.org/10.5194/hess-2022-330
Preprint. Discussion started: 4 October 2022

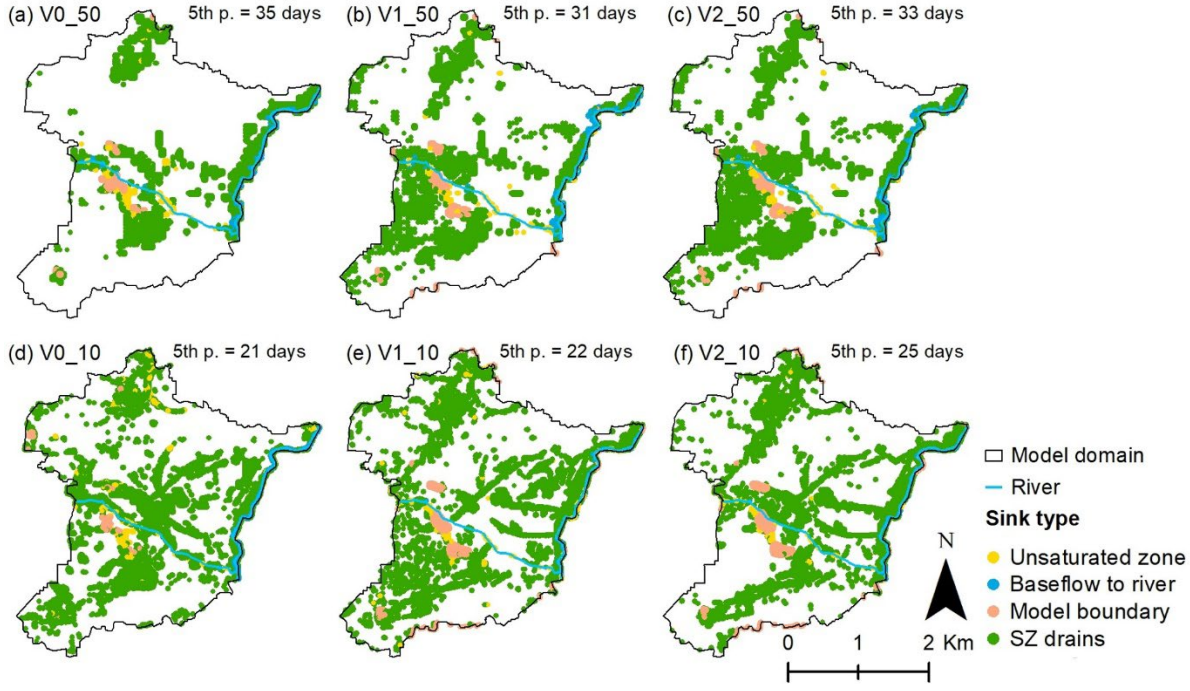

480 **Figure 12. Release locations of particles that are within the 5th percentile of the travel times to sinks and their end sink types. SZ drains stand for saturated zone drains and includes leaking sewers.**

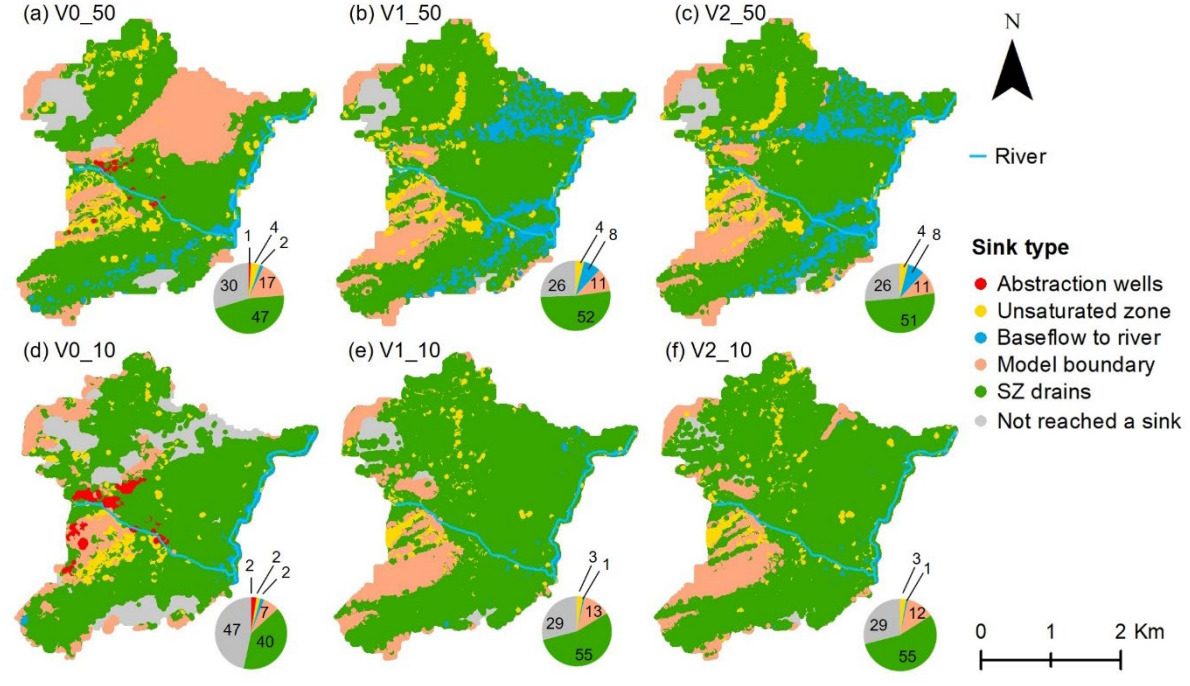

Figure 13. Start location of all released particles and their end sink. Pie diagrams show the percentage of particles ending up in the different sinks.

https://doi.org/10.5194/hess-2022-330
Preprint. Discussion started: 4 October 2022


Hydrology and Earth System Sciences
Discussions

In Figure 13 the starting locations for all particles released within the model area are shown and divided into the different sinks the particles discharge to (opposite Figure 12 where only the fastest 5th percentile of particles are shown). Pie diagrams of the percentages of the particles captured by the different sinks are shown as inserts in the figure.

The results presented in Figure 13 and Table 4 indicate that the urban geology incorporated in V1 and V2 introduces major changes in the groundwater pathways. Here, a higher percentage of the particles is captured by the drainage system, while the computational grid size also impacts the distribution of particles among the sinks. In all models, 25-30% of the particles do not reach a sink within 200 years, except for V0_10 where 47% of the particles do not reach a sink. As seen in Figure 13, it is only in the V0 models that the released particles were captured by the abstraction wells.

5 Discussion

The effect of the geological configuration and grid size was analyzed based on their simulation of high-water levels, the 95th percentile, and particle tracking. The level of detail in the voxel models depended on both the available data and their quality as well as the spatial resolution of the model. The knowledge of the properties of the infill as well as the dimensions (e.g. exact size of trenches) of the anthropogenic structures was limited, nevertheless, 7% of the volume in the voxel models was modified compared to the base model V0.

The calibration of the six hydrological models resulted in an almost similar fit to the observation data both in terms of mean error for head and stream discharge and in terms of the yearly head dynamics, see Figure 6, 7, and 8. Yet, for the V1_10 and V2_10 the RMSE_h was 20 cm lower than for the other models. The better fit obtained for the V1_10 and V2_10 models is most likely due to the better description and evolution of the shallow geology. In the objective function for head, all measurements were given the same weight, but the RMSE_h of the shallow wells was generally better than for the deeper in the V1 and V2 models (than the V0 models). The RMSE_h for the V1 and V2 models in 10 m resolution was 1.7 m and 1.0 m, respectively, for the deep and shallow wells.

By using preferred value regularization in the calibration process the parameter uncertainty was reduced. We considered the preferred parameter values to be realistic and therefore the parameter optimization was constrained such that unrealistic parameter estimates were avoided for the parameters that were less informed by observations as argued by (Doherty, 2015). The effect of the regularization was evident for, e.g., the root depth of grass ($dr_{,grass}$) for which unrealistic estimates were obtained without regularization. The parameter estimation with preferred value regularization thus constrained the calibration for parameters, which were poorly informed by the observation data, even though the relative error variance for these parameters was not reduced. Moreover, as a side effect of the regularization the resulting six models remained comparable in the sense that the parameter values remain within the same order of magnitude across the different models, see Figure 9.

The largest contrast in terms of estimated parameter values was found between the V0 model and the two urban models. The results from the parameter identifiability analysis showed that the parameters, which were more informed by observations

https://doi.org/10.5194/hess-2022-330
Preprint. Discussion started: 4 October 2022


Hydrology and Earth System Sciences
Discussions

were changed from the base model to the two urban models. This is especially clear for parameter $K_{qs2,h}$, which showed fairly warm colors in the V0 model while cold colors are dominating in the V1 and V2 models. This is mainly because of the introduction of the sand/clay classes, which replaced much of the quaternary sand layers, K_{qs}.

Furthermore, the analysis of the resulting parameter estimates and their identifiability indicates that when the models are run with a finer horizontal resolution (10 m) the models become more sensitive to the hydraulic conductivity parameters, which have either high or low conductivity even though they are only locally present in the model. The lower sensitivity towards geological heterogeneity when the models represent a coarser spatial resolution is presumably because of their inability to resolve the heterogeneity.

In both 50 and 10 m resolutions, the urban geology models V1 and V2 perform equally well and similar groundwater levels and travel times were obtained. This suggests that including information from geotechnical boreholes and soil data in model V2, as opposed to V1, did not lead to a noticeable change in the hydrological simulations. This could be because the shallow groundwater levels primarily were simulated below the 1 m, which was the depth to which the soil map was represented. The largest change in hydrological simulations occurred from V0 to V1, when the urban infrastructure data was included in the geological model, particularly utility trenches and road and railways build-up materials. The shallow basements did not show a noticeable impact on the simulation, only the very deep hospital basement (10m) impacted the simulation of the depth to the water table, Figure 11. The reason why urban infrastructure has an impact is due to the interconnection created between roads and utility trenches and coupled with the relatively high hydraulic conductivity of the build-up and backfill materials compared to the surrounding geological settings. The particle tracking results from both V1_50, V1_10, V2_50, and V2_10 indicate that these conduits with high hydraulic conductivity create local preferential flow paths.

It was assumed that the entire sewer system was leaky and thus acted as a drainage system as well. In consequence, drains in the saturated zone were by far the most dominant sink to the shallow groundwater, Figure 12 and Figure 13. Although this assumption may be on the extreme side, groundwater seeping into the sewers is a common problem and leads to excessive water treatment in areas with shallow groundwater. On the other hand, in cases where such sewers are renovated, the water table may raise and trigger water seeping into basements or a periodical groundwater table above the terrain. The six model simulations would most likely be different if the sewer system was not leaking. The preferential flow paths would still be present, but the water in those locations would not be drained.

The computational grid resolution affected the simulation results both for the groundwater levels and the particle tracking. The 95th percentile of the simulated water table depth by the six models showed that the local variation in the model domain was smeared out in the 50 m models as compared to the variations in the 10 m models. The urban models V1_10 and V2_10 provide a much more refined spatial simulation compared to both V0_10 and V0_50. This suggests that a high-resolution hydrological model can benefit from a detailed urban geological model, while a coarse resolution hydrological model with a resolution coarser than the scale of the subsurface infrastructures smears out the effect of local flow pathways. This is in agreement with (Hibbs and Sharp, 2012) who also found that a fine spatial resolution is required to effectively utilize data on

https://doi.org/10.5194/hess-2022-330
Preprint. Discussion started: 4 October 2022

subsurface constructions such as trenches of water and sewer pipes, storm drains and other utility systems and hereby consider fast flow conduits generated by such structures.

The particle tracking showed that in models V1_10, V1_50, V2_10, and V2_50, recharge did not reach the deeper groundwater system. The shallow groundwater has near-surface flow paths and discharges to rivers, urban drainage systems, ponds, and lakes, see Figure 12 and Figure 13. This is as previously stated most likely due to the interconnected subsurface infrastructures that cause preferential flow paths.

Comparing the particle tracking results across geological conceptualizations and spatial resolutions it appears that the former is more important than the latter, and the results thus suggest that urban geology affects groundwater recharge. This has also been documented by Fletcher et al. (2013) among others. However, in these studies, the groundwater table is located below the sewer system and therefore receives indirect recharge from leaky water pipes, while in this study it was found that the inclusion of the urban geology reduced recharge to deeper groundwater aquifers. This could have both a negative and positive effect on the deeper groundwater; negative in the sense that less recharge is available for the deeper groundwater resources, but positive in the sense that the deeper groundwater is not impacted by potentially contaminated water in shallow aquifers below the city.

6 Conclusion

This study examined the impacts of anthropogenic urban geology and spatial resolution on the simulation of shallow groundwater at the city scale. The sensitivity of geological detail was analyzed by applying three geological models as input to three otherwise identical hydrological models, while the effect of spatial resolution was analyzed by varying the computational grid size of the hydrological models.

All the models were calibrated individually against the head observations from both shallow groundwater, deep aquifers, and stream discharge with the use of preferred value regularization. This gave a good fit to the observation data set for all models. Meanwhile, this calibration approach constrained the parameters, which were less informed by observations to achieve reasonable parameter values, which were in the same order of magnitude across the six hydrological model versions.

The results of the stepwise development of the geological model and test of its effect on the hydrogeological simulation showed that the representation of the anthropogenic urban geology did not alter the depth of the water table to a large degree, yet it altered the flow paths and travel time of the shallow groundwater. In terms of geological detail, the results showed that the largest impact on the simulation of the shallow groundwater was caused by the subsurface infrastructures; specifically, utility trenches and the build-up material of roads and railways since these interconnected structures acted as preferential pathways for the shallow groundwater. The anthropogenic geology affected both the simulated flow path and the residence time of the water particles. Since the hydrological models assumed a leaky sewer system, the results from this study suggest that the presence of these preferential flow paths also impacted the simulated recharge of groundwater. The sewer system

and drains in the less urbanized areas became a much larger sink of groundwater when these preferential flow paths were represented.

In terms of computation grid resolution, the largest impact of representing the urban geology was seen in the finer computational grid resolution of 10 m of the hydrological model compared to the 50 m resolution of the hydrological model, since the model in 50 m resolution smeared out the effect of the local subsurface infrastructure preferential flow paths. Thus, the results from this study indicate that it is important to consider the dimension and hydrological properties of the urban subsurface infrastructures and subsurface buildings as they affect the groundwater levels and flow paths and hence also the sinks and recharge of the water to deeper aquifers and particles residence time in the aquifers.

In this study, a difference between the baseline model V0 and the models with detailed urban geology V1 and V2 was evident despite the anthropogenic geology only represented 7 % of the total voxel model. This indicates that even though urban structures only alter a fraction of the shallow surface it may cause a significant impact on the hydrogeology which can change water levels, flow paths, end sinks and travel time distributions to the sinks.

Author contribution: AL and JK designed and executed the hydrological modeling work. AL led the data analysis and wrote the initial draft of the paper. MHM and PS designed and executed the geological modeling, KHJ, TOS and JK contributed scientifically to the modeling and data analysis. All authors contributed to the paper by providing comments, editing, and suggestions.

Competing interests: The authors declare that they have no conflict of interest.

Acknowledgments: The work was carried out as part of the SUBWATER project with financial support granted by the Danish Geocenter, VandCenter Syd A/S, Southern Region of Denmark, and the Municipality of Odense.

References

Abbott, M. B., Bathurst, J. C., Cunge, J. A., O'Connell, P. E., and Rasmussen, J.: An introduction to the European Hydrological System — Systeme Hydrologique Europeen, "SHE", 1: History and philosophy of a physically-based, distributed modelling system, J. Hydrol., 87, 45–59, https://doi.org/10.1016/0022-1694(86)90114-9, 1986a.

Abbott, M. B., Bathurst, J. C., Cunge, J. A., O'Connell, P. E., and Rasmussen, J.: An introduction to the European Hydrological System — Systeme Hydrologique Europeen, "SHE", 2: Structure of a physically-based, distributed modelling system, J. Hydrol., 87, 61–77, https://doi.org/10.1016/0022-1694(86)90115-0, 1986b.

Andersen, T. R., Poulsen, S. E., Pagola, M. A., and Medhus, A. B.: Geophysical mapping and 3D geological modelling to support urban planning: A case study from Vejle, Denmark, J. Appl. Geophys., 180, 104130, https://doi.org/10.1016/j.jappgeo.2020.104130, 2020.

Attard, G., Rossier, Y., Winiarski, T., Cuvillier, L., and Eisenlohr, L.: Deterministic modelling of the cumulative impacts of underground structures on urban groundwater flow and the definition of a potential state of urban groundwater flow: example of Lyon, France, Hydrogeol. J., 24, 1213–1229, https://doi.org/10.1007/s10040-016-1385-z, 2016a.

Attard, G., Winiarski, T., Rossier, Y., and Eisenlohr, L.: Revue: Impact des structures du sous-sol sur les écoulements des eaux souterraines en milieu urbain, Hydrogeol. J., 24, 5–19, https://doi.org/10.1007/s10040-015-1317-3, 2016b.

Attard, G., Rossier, Y., and Eisenlohr, L.: Urban groundwater age modeling under unconfined condition - Impact of underground structures on groundwater age: Evidence of a piston effect, J. Hydrol., 535, 652–661, https://doi.org/10.1016/j.jhydrol.2016.02.034, 2016c.

Attard, G., Rossier, Y., and Eisenlohr, L.: Underground structures increasing the intrinsic vulnerability of urban groundwater: Sensitivity analysis and development of an empirical law based on a groundwater age modelling approach, J. Hydrol., 552, 460–473, https://doi.org/10.1016/j.jhydrol.2017.07.013, 2017.

Berthier, E., Andrieu, H., and Creutin, J. D.: The role of soil in the generation of urban runoff: development and evaluation of a 2D model, J. Hydrol., 299, 252–266, https://doi.org/10.1016/j.jhydrol.2004.08.008, 2004.

Birks, D., Whittall, S., Savill, I., Younger, P. L., and Parkin, G.: Groundwater cooling of a large building using a shallow alluvial aquifer in Central London, Q. J. Eng. Geol. Hydrogeol., 46, 189–202, https://doi.org/10.1144/qjegh2012-059, 2013.

Butts, M. and Graham, D.: Flexible Integrated Watershed Modeling with MIKE SHE, Watershed Model., 245–271, https://doi.org/10.1201/9781420037432.ch10, 2005.

Culshaw, M. G. and Price, S. J.: The 2010 Hans Cloos lecture, Bull. Eng. Geol. Environ., 70, 333–376, https://doi.org/10.1007/s10064-011-0377-4, 2011.

Danish Meteorological Institute (DMI): Climate data - Precipitation, ETref*0.95 and Temperature, 2021.

Danish National Agency for Data Supply and Infrastructure: Digital Terrain Model 10m, https://download.kortforsyningen.dk/, 2019.

DHI: MIKE SHE 2020 User Guide and Reference Manual, 822 pp., 2020.

Doherty, J.: Calibration and Uncertainty Analysis for Complex Environmental Models, 2015.

Doherty, J.: PEST Model-Independent Parameter Estimation, User Manual part II, 2016a.

Doherty, J.: PEST Model-Independent Parameter Estimation User Maunal Part I, 2016b.

Farr, G. J., Patton, A. M., Boon, D. P., James, D. R., Williams, B., and Schofield, D. I.: Mapping shallow urban groundwater temperatures, a case study from Cardiff, UK, Q. J. Eng. Geol. Hydrogeol., 50, 187–198, https://doi.org/10.1144/qjegh2016-058, 2017.

Fletcher, T. D., Andrieu, H., and Hamel, P.: Understanding, management and modelling of urban hydrology and its consequences for receiving waters: A state of the art, Adv. Water Resour., 51, 261–279, https://doi.org/10.1016/j.advwatres.2012.09.001, 2013.

Ford, J. R., Price, S. J., Cooper, A. H., and Waters, C. N.: An assessment of lithostratigraphy for anthropogenic deposits, Geol. Soc. Spec. Publ., 395, 55–89, https://doi.org/10.1144/SP395.12, 2014.

Han, D., Currell, M. J., Cao, G., and Hall, B.: Alterations to groundwater recharge due to anthropogenic landscape change, J. Hydrol., 554, 545–557, https://doi.org/10.1016/j.jhydrol.2017.09.018, 2017.

Hibbs, B. J. and Sharp, J. M.: Hydrogeological impacts of urbanization, Environ. Eng. Geosci., 18, 3–24, https://doi.org/10.2113/gseegeosci.18.1.3, 2012.

Hutchins, M. G., McGrane, S. J., Miller, J. D., Hagen-Zanker, A., Kjeldsen, T. R., Dadson, S. J., and Rowland, C. S.: Integrated modeling in urban hydrology: reviewing the role of monitoring technology in overcoming the issue of 'big data' requirements, 4, https://doi.org/10.1002/wat2.1177, 2017.

Jakobsen, P. R. and Tougaard, L.: Geomorfologisk kort over Syd- og Østdanmark, version2, https://data.geus.dk/geusmap/?mapname=denmark#baslay=baseMapDa&optlay=&extent=290273.4254273991,6075492.263147449,843727.9711775389,6356543.399661193, 2018.

Jakobsen, P. R., Tougaard, L., and Anthonsen, K. L.: Danmarks Digitale Jordartskort 1:25 000 version 6.0 - ArcGIS og QGIS, https://doi.org/doi/10.22008/FK2/XAFCRS, 2022.

Kidmose, J. and Sonnenborg, T. O.: Fælles grundvand - Fælles ansvar: WP2 Hydrologisk model, GEUS, https://doi.org/10.22008/gpub/32579, 2018.

Kidmose, J., Troldborg, L., Refsgaard, J. C., and Bischoff, N.: Coupling of a distributed hydrological model with an urban storm water model for impact analysis of forced infiltration, J. Hydrol., 525, 506–520, https://doi.org/10.1016/j.jhydrol.2015.04.007, 2015.

Laursen, G. and Linderberg, J.: Odense - A City with Water Issues, Procedia Eng., 209, 104–118, https://doi.org/10.1016/j.proeng.2017.11.136, 2017.

Lerner, D. N.: Groundwater recharge in urban areas, Atmos. Environ. Part B, Urban Atmos., 24, 29–33, https://doi.org/10.1016/0957-1272(90)90006-G, 1990.

Lerner, D. N.: Identifying and quantifying urban recharge: A review, Hydrogeol. J., 10, 143–152, https://doi.org/10.1007/s10040-001-0177-1, 2002.

Levin, G., Iosub, C.-I., Jepsen, M. R., Blemmer, M. K., and Nielsen, M. R.: Basemap: technical documentation of a model for elaboration of a land-use and land-cover map for Denmark, Technical Report from DCE – Danish Centre for Environment and Energy, 64 pp., 2012.

Locatelli, L., Mark, O., Mikkelsen, P. S., Arnbjerg-Nielsen, K., Deletic, A., Roldin, M., and Binning, P. J.: Hydrologic impact of urbanization with extensive stormwater infiltration, J. Hydrol., 544, 524–537, https://doi.org/10.1016/j.jhydrol.2016.11.030, 2017.

Lundy, L. and Wade, R.: Integrating sciences to sustain urban ecosystem services, Prog. Phys. Geogr., 35, 653–669, https://doi.org/10.1177/0309133311422464, 2011.

McGrane, S. J.: Impacts of urbanisation on hydrological and water quality dynamics, and urban water management: a review, Hydrol. Sci. J., 61, 2295–2311, https://doi.org/10.1080/02626667.2015.1128084, 2016.

Mielby, S. and Henriksen, H. J.: Hydrogeological studies integrating the climate, freshwater cycle, and catchment geography

for the benefit of urban resilience and sustainability, 12, https://doi.org/10.3390/w12123324, 2020.

Mielby, S. and Sandersen, P. B. E.: Development of a 3D geological/hydrogeological model targeted at sustainable management of the urban water cycle in Odense City, Denmark, Procedia Eng., 209, 75–82, https://doi.org/10.1016/j.proeng.2017.11.132, 2017.

Mitchell, V. G.: Applying integrated urban water management concepts: A review of Australian experience, Environ. Manage., 37, 589–605, https://doi.org/10.1007/s00267-004-0252-1, 2006.

Odense Kommune: Odense kommune Spildevandsplan 2011-2022, 1–75 pp., 2011.

Petrosino, P., Claudia Angrisani, A., Barra, D., Donadio, C., Aiello, G., Allocca, V., Coda, S., De Vita, P., Jicha, B. R., and Calcaterra, D.: Multiproxy approach to urban geology of the historical center of Naples, Italy, Quat. Int., 577, 147–165, https://doi.org/10.1016/j.quaint.2020.12.043, 2021.

Pophillat, W., Sage, J., Rodriguez, F., and Braud, I.: Dealing with shallow groundwater contexts for the modelling of urban hydrology – A simplified approach to represent interactions between surface hydrology, groundwater and underground structures in hydrological models, Environ. Model. Softw., 144, https://doi.org/10.1016/j.envsoft.2021.105144, 2021.

Pophillat, W., Sage, J., Rodriguez, F., and Braud, I.: Consequences of interactions between stormwater infiltration systems , shallow groundwater and underground structures at the neighborhood scale, Urban Water J., 00, 1–12, https://doi.org/10.1080/1573062X.2022.2090382, 2022.

Rodriguez, F., Andrieu, H., and Morena, F.: A distributed hydrological model for urbanized areas - Model development and application to case studies, J. Hydrol., 351, 268–287, https://doi.org/10.1016/j.jhydrol.2007.12.007, 2008.

Salvadore, E., Bronders, J., and Batelaan, O.: Hydrological modelling of urbanized catchments: A review and future directions, J. Hydrol., 529, 62–81, https://doi.org/10.1016/j.jhydrol.2015.06.028, 2015.

Sandersen, P. B. E. and Jørgensen, F.: Kortlægning af begravede dale i Danmark. Opdatering 2010-2015. Bind 2. Lokalitetsbeskrivelser (Særudgivelse)., De Nationale Geologiske Undersøgelser for Danmark og Grønland, Denmark, 2016.

Sandersen, P. B. E. and Kallesøe, A. J.: Odense Vest - 3D geologisk /hydrostratigrafisk detailmodellering, GEUS, Copenhagen, https://doi.org/10.22008/gpub/32521, 2017.

Schirmer, M., Leschik, S., and Musolff, A.: Current research in urban hydrogeology - A review, Adv. Water Resour., 51, 280–291, https://doi.org/10.1016/j.advwatres.2012.06.015, 2013.

Stisen, S., Ondracek, M., Troldborg, L., Schneider, R. J. M., and van Til, M. J.: National Water Resource Model - Construction and calibration of the DK-model2019 (in Danish), 125 pp., 2019.

Troldborg, L., Ondracek, M., Koch, J., Kidmose, J., and Refsgaard, J. C.: Quantifying stratigraphic uncertainty in groundwater modelling for infrastructure design, Hydrogeol. J., 29, 1075–1089, https://doi.org/10.1007/s10040-021-02303-5, 2021.

Tubau, I., Vázquez-Suñé, E., Carrera, J., Valhondo, C., and Criollo, R.: Quantification of groundwater recharge in urban environments, Sci. Total Environ., 592, 391–402, https://doi.org/10.1016/j.scitotenv.2017.03.118, 2017.

United Nations: World Urbanization Prospects : The 2018 Revision, New York, 2 pp., 2018.

https://doi.org/10.5194/hess-2022-330
Preprint. Discussion started: 4 October 2022


Hydrology and Earth System Sciences
Discussions

715 Vandcenter Syd A/S: MIKE Urban catchments, 2019a.

Vandcenter Syd A/S: Odense Sewer Network, 2019b.

Vandcenter Syd A/S: Hydraulic head observations and abstraction timeseries, 2021.

Vázquez-Suñé, E., Carrera, J., Tubau, I., Sánchez-Vila, X., and Soler, A.: An approach to identify urban groundwater recharge, Hydrol. Earth Syst. Sci., 14, 2085–2097, https://doi.org/10.5194/hess-14-2085-2010, 2010.

720 Vázquez-Suñé, E., Marazuela, M. Á., Velasco, V., Diviu, M., Pérez-Estaún, A., and Álvarez-Marrón, J.: A geological model for the management of subsurface data in the urban environment of Barcelona and surrounding area, 7, 1317–1329, https://doi.org/10.5194/se-7-1317-2016, 2016.

Yang, Y., Lerner, D. N., Barrett, M. H., and Tellam, J. H.: Quantification of groundwater recharge in the city of Nottingham, UK, Environ. Geol., 38, 183–198, https://doi.org/10.1007/s002540050414, 1999.

725